Musgrave, R., Russell, A., Hayward, D., Whittell, G., Lawrence, P., Gates, P., ... Manners, I. (2017). Main-chain metallopolymers at the static–dynamic boundary based on nickelocene. *Nature Chemistry*, *9*, 743-750. https://doi.org/10.1038/nchem.2743

Main Chain Metallopolymers at the Static-Dynamic Boundary Based on Nickelocene

Rebecca A. Musgrave,[1] Andrew D. Russell,[1] Dominic W. Hayward,[1] George R. Whittell,[1] Paul G. Lawrence,[1] Paul. J. Gates,[1] Jennifer C. Green[2] and Ian Manners[1,*]

[1]School of Chemistry, University of Bristol, Cantock's Close, Bristol, BS8 1TS, UK.

[2]Department of Chemistry, University of Oxford, Chemical Research Laboratory, Mansfield Road, Oxford, OX1 3TA, UK.

Abstract

Interactions between metal ions and ligands in metal-containing polymers involve two bonding extremes: persistent covalent bonding, where the polymers are essentially static in nature, or labile coordination bonding, which leads to dynamic supramolecular materials. Main chain polymetallocenes based on ferrocene and cobaltocene fall into the former category due to the presence of strong metal–cyclopentadienyl bonds. Herein we describe a main chain polynickelocene formed by ring-opening polymerization of a moderately strained [3]nickelocenophane monomer, that can be switched between static and dynamic states as a result of the relatively weak Ni–cyclopentadienyl ligand interactions. This is illustrated by the observation that, at low concentration or at elevated temperature in a coordinating or polar solvent, depolymerization of the polynickelocene occurs. A study of this dynamic polymer-monomer equilibrium by ^{1}H NMR spectroscopy allowed for determination of the associated thermodynamic parameters. Microrheology data, however, indicated that under similar conditions the polynickelocene is considered to be static on the shorter, rheological timescale.

Introduction

Metallopolymers combine the inherent functionality of metal centres with the mechanical properties and processing advantages of macromolecules.[1-3] In many cases the binding of the metal ions within the ligating 1D architecture is strong and static in nature, leading to materials with a range of useful properties but which resemble traditional covalent polymers. In contrast, the use of weak and labile metal-ligand interactions leads to metallosupramolecular materials which exhibit dynamic behaviour.[4, 5] This diversity in structure and dynamics has facilitated a myriad of applications that include self-healing,[6, 7] light emission,[8, 9] photovoltaics,[10, 11] stimuli-responsive behaviour,[12, 13] catalysis,[14] information storage,[15] antibacterial activity,[16] and nanopatterning.[17-19]

Main-chain polymetallocenes based on ferrocene, such as polyferrocenylsilanes (PFSs) (Fig. 1a), represent a well-studied field of metallopolymers and exemplify a static system with strong, persistent covalent Fe–Cp (Cp = cyclopentadienyl) interactions. These materials contain Fe centres with 18 valence electrons (VEs) and are prepared via the ring-opening polymerization (ROP) of strained [1]- or [2]ferrocenophane monomeric precursors. These monomers are examples of [*n*]metallocenophanes (**1**, Fig. 1b) where the inherent ring strain acts as a thermodynamic driving force for the ROP process.[20, 21] This strain can be quantified by the angle between the Cp ring planes (α) and several other structural parameters (Fig. 1b). Polymetallocenes and related materials based on metals other than iron are less common but are also accessible via ROP of strained precursors.[20, 22-24] For example, dicarba[2]cobaltocenophane **2** (Fig. 1c), containing a 19 VE Co centre, undergoes thermal ROP and subsequent oxidation to yield poly(cobaltoceniumethylene) ([PCE]$^+$), a water-soluble polyelectrolyte with main-chain cobaltocenium units (Fig. 1a).[25] These materials contain cobaltocenium units with 18 VE which feature strong Co–Cp bonds and also exhibit static behaviour.[26]

Diamagnetic polymetallocenes such as PFS and $[PCE]^+$ feature repeat units with 18 VE metal centres. In contrast, paramagnetic analogues of these polymetallocenes such as 17 VE $[PFS]^+$ and 19 VE PCE (Fig. 1a) are insoluble in common organic solvents, and the preparation of soluble polymetallocenes with unpaired electrons represents an undeveloped field, with very limited examples of these types of polymers.[27-29]

Nickelocene, which possesses 20 VEs and a triplet ($^3A_2$) ground state, accommodates two electrons in antibonding orbitals. This results in elongation of the Ni–Cp bond (Ni–Cp_{cent} distance = 1.817(1) Å), relative to the corresponding values found in cobaltocene (19 VE, Co–Cp_{cent} = 1.726(1) Å) and ferrocene (18 VE, Fe–Cp_{cent} = 1.643(2) Å), and subsequent weakening.[30] As a result of the trend in M–Cp bond length, the tilt angle, α, of structurally analogous [*n*]metallocenophanes increases from Fe to Co to Ni. For example, tilt increases from the tricarba[3]ferrocenophane **3** (α = 10.3°) to the tricarba[3]cobaltocenophane **4** (α = 12.0°), but both of these species resist attempted ROP (Fig. 1c). In contrast, we recently showed that tricarba[3]nickelocenophane (**5**) is significantly more tilted (α = 16.6°) and undergoes spontaneous ROP in pyridine at ambient temperature to yield the soluble magnetic main chain polynickelocene **7**, containing S = 1 spin centres.[29] This material was shown to be of high molar mass (weight average molar mass M_w = ca. 40,000 g mol^{-1}) based on dynamic light scattering (DLS) studies in THF, and analysis by MALDI-TOF indicated the presence of both cyclic and linear components. Paramagnetic polynickelocene **7** was also found to exhibit significant antiferromagnetic spin-spin interactions, with evidence for intramolecular spin-spin coupling along the polymer chains.[29] Herein we demonstrate that, as a consequence of the weaker Ni–Cp bonds (M–Cp dissociation energy is 250 kJ mol^{-1} for nickelocene vs. 305 kJ mol^{-1} for ferrocene),[31] polynickelocene **7** can exist in either a static or labile state, and in the latter case forms a dynamic equilibrium with monomer **5** and small amounts of cyclic oligomers $\mathbf{6_x}$, under a range of conditions (Fig. 1d).

Results and Discussion

In order to obtain more detailed insight into the unusual solution polymerization of **5** in the absence of an externally added initiator, we studied the ROP (0.79 M **5**, 25 °C) in d_5-pyridine by paramagnetic ^{1}H NMR spectroscopy (Supplementary Fig. 1). The solution changed from the characteristic blue colour of **5** to green as **7** gradually formed. Broad singlets were observed in paramagnetic regions of the ^{1}H NMR spectrum after 24 h, which could be assigned to the Cp ring protons of both polymer **7** (δ = –250.0 ppm (η^5-C_5H_4)) and monomer **5** (δ = –245.4 and –270.9 ppm (α and β η^5-C_5H_4 protons, respectively)). Protons at the α and β positions in the propyl spacer of the polymer **7** were also observed at 176.9 and 9.6 ppm respectively. The β protons of monomer **5** were observed at –29.0 ppm (α protons are not observed, as reported previously).[29] Integration of the shifts corresponding to Cp protons at high field after 24 h indicated that ca. 69% of the [3]nickelocenophane monomer **5** had been converted to polynickelocene **7**. Extension of the reaction time to 7 days with *in situ* ^{1}H NMR spectroscopic analysis led to only a slight further conversion of **5** to **7**, suggesting that the polymerization is essentially complete after 24 h and that an equilibrium between monomer and polymer was present. In addition to shifts assigned to either monomer or polymer, four small resonances were observed in the region of polymer α-CH_2 protons, at 266.8, 197.3, 185.2 and 181.6 ppm. We assign these to cyclic oligomeric species $\mathbf{6_2}$–$\mathbf{6_5}$ (dimer, trimer, tetramer and pentamer respectively: see below).

The percentage monomer conversion was therefore similarly investigated as a function of time over five additional concentrations (range: 0.04 – 1.31 M) to yield a series of six polynickelocene samples in total, $\mathbf{7_a}$–$\mathbf{7_f}$. The ^{1}H NMR spectra for the formation of $\mathbf{7_a}$–$\mathbf{7_f}$ from **5** after 48 h in d_5-pyridine are shown in Fig. 2. ^{1}H NMR spectroscopic analysis revealed that performing the ROP at higher concentrations increased both the conversion of monomer (determined by integration of Cp resonances in the ^{1}H NMR spectrum), and the yield of

polymer isolated after precipitation (Table 1). The discrepancies between the monomer conversion observed by ^{1}H NMR spectroscopy and the yield of isolated polymer presumably result from the formation of cyclic oligomeric species, (at 266.8, 197.3, 185.2 and 181.6 ppm, for $\mathbf{6_2}$–$\mathbf{6_5}$, respectively), which do not precipitate from solution upon work up. These cyclic oligomer resonances are particularly evident in the ^{1}H NMR spectrum of the polymerization mixture for the case of $\mathbf{7_c}$ (0.44 M) (Fig. 3a). After the first precipitation of polymer $\mathbf{7_c}$, an enhancement of these resonances in the ^{1}H NMR spectrum of the supernatant washings was observed (Fig. 3b), in addition to observation of resonances for $\mathbf{6_6}$, $\mathbf{6_7}$ and $\mathbf{6_8}$ (at 180.0, 179.4 and 178.9 ppm respectively), indicating the hexane-solubility of these oligomeric species. Electrospray ionization mass spectrometry (ESI-MS) also provided evidence for cyclic oligomers $\mathbf{6_2}$, $\mathbf{6_3}$ and $\mathbf{6_4}$ (Supplementary Figs 2−6) similar in nature to reported cyclic oligomeric ferrocenes.[32, 33] The cyclic vs. linear nature of these oligomers is highly likely, as no end groups were detected by ^{1}H NMR or by ESI-MS. The overall observed concentration dependence confirmed that tricarba[3]nickelocenophane **5** and polynickelocene **7** exist in dynamic equilibrium in pyridine solution. The presence of cyclic species in reversible polymerisations is known for several systems (e.g. polysiloxanes, polyesters, polyamides).[34, 35]

The solvent dependency of the equilibrium between **5** and **7** has been investigated by a number of polymerization and depolymerization experiments, with initial equilibration rates found to be in the order pyridine > CH_2Cl_2 > THF ≈ 1,2-difluorobenzene > benzene ≈ toluene (Supplementary Figs 7 and 8). The equilibration process in benzene and toluene is particularly slow at ambient temperature and polynickelocene **7** can be regarded as essentially stable and static under these conditions (only ca. 15% retroconversion of **7** to **5** was detected in toluene even after 1 month). The mechanism for the equilibration process in donor solvents presumably involves cleavage of the Ni–Cp bond and coordination of solvent to the resulting

14 VE nickel-centred cation (see schemes in Supplementary Figs 9 and 10), with propagation occurring by either a chain growth or step growth mechanism (or a combination of both). Consistent with the proposed mechanism, coordination of two-electron donors such as N-heterocyclic carbenes and monodentate phosphines is well-known for nickelocene,[36, 37] with an associated haptotropic Cp ring shift from η^5 to η^1 coordination at nickel. Substitution of one Cp ring in nickelocene has also been observed using neutral ligands such as borolenes,[38] azaphospholes,[39] cyanoalkynes, and trifunctional phosphines.[40]

Although ^{1}H NMR spectroscopy provided insight into the monomer-polymer equilibrium, this approach cannot be used to determine the molar mass of polymer **7** as a function of concentration as no end groups were evident. As the equilibration was found to be very slow in toluene, comparative values of M_w were determined in this solvent. Samples of polymers **7$_a$**, **7$_b$** and **7$_c$** in pyridine at concentrations of 1.31 M, 0.79 M, and 0.44 M, were prepared and isolated and each material was then examined by DLS at a concentration of 1 mg mL^{-1} in toluene (Supplementary Figs 11–13). As anticipated, the value of the hydrodynamic radius, R_h, for **7$_c$** (3.2 nm) was found to be significantly smaller than those of both **7$_b$** and **7$_a$**, which were similar within experimental error (6.3 and 5.7 nm respectively (Table 1)) and were affected by solubility issues (see Supplementary Information, section 5 for details). The smaller value for **7$_c$** is consistent with the expectation that, as the concentration of the ROP reaction decreases, the molar mass of the resulting polymer should also decrease.[41] The molar masses calculated from R_h values determined by DLS (Table 1 and Supplementary Table 1) are relative to calibrants. We therefore also determined the values of M_w using Small Angle X-ray Scattering (SAXS), which is an absolute method (see Supplementary Figs 14–16 and Supplementary Information, section 6 for details).[42] This gave values for **7$_b$** and **7$_c$** of 20,000 g mol^{-1} and 6,400 g mol^{-1} (Table 1), significantly lower than the relative values estimated

from R_h data, but in the expected order based on initial monomer concentration (see Supplementary Information, section 6 for details).

Several addition polymerizations of organic monomers have been shown to be reversible under certain conditions that permit equilibration of polymer and monomer, and these are exemplified by the cases of methyl methacrylate, α-methylstyrene and isobutylene.[43-46] Examples of reversible ROP processes are also known for organic cyclic species, for example THF in the presence of Lewis acids and cyclopentene in the presence of certain metal alkylidene complexes.[41, 47, 48] Most of the known reversible polymerizations are characterized by small, favourable (negative) values of ΔH and unfavourable (negative) values of ΔS. As the temperature of such a polymerization increases, the importance of the entropic TΔS term to the overall free energy of the system, ΔG, also increases and depolymerization is favoured. Other examples, such as the 8-membered inorganic rings S_8 and $[Me_2SiO]_4$ are highly unusual in that ΔS is favourable (positive) and depolymerization is favoured at lower temperature.[35] Detailed studies of reversible polymerizations as a function of temperature allowed the key thermodynamic parameters ΔH and ΔS to be determined. The reversible equilibration between **5** and **7** represents a unique example of a ROP system involving a transition metal centre. Therefore to provide additional fundamental insight, we explored the influence of temperature on the position of equilibrium between these two species.

The polymerization of monomer **5** was conducted under ROP conditions (d_5-pyridine, 0.44 M, 24 h) that, at room temperature (20 °C), result in ca. 50% monomer conversion at equilibrium (conditions used to form sample **7c**). The mixture was equilibrated for 24 h at a range of different temperatures from –5 to 60 °C, and was then analysed by *in situ* ^{1}H NMR spectroscopy (Fig. 4). The results (summarized in Supplementary Table 2) confirmed that temperature significantly affects the position of the equilibrium, with monomer **5** favoured at

high temperatures and polymer **7** favoured at low temperatures (e.g. at 60 °C, only 29% conversion to **7** was detected, whereas at –5 °C, conversion to **7** increased to 70%).

This dynamic equilibrium between monomer **5** and polymer **7** was analysed using equations 1–3.[41]

$$\ln[M]_c = \frac{\Delta H^0_{ROP}}{RT} - \frac{\Delta S^0_{ROP}}{R} \qquad (1)$$

$$\Delta G_{ROP} = \Delta G^0_{ROP} + RT\ln K \qquad (2)$$

$$T_c = \frac{\Delta H^0_{ROP}}{\Delta S^0_{ROP} + R\ln[M]_c} \qquad (3)$$

Equation 1, an adaption of the Van't Hoff equation, allows values of ΔH^0_{ROP} and ΔS^0_{ROP} to be determined from a plot of equilibrium monomer concentration $[M]_c$ against reciprocal temperature (Supplementary Table 3, Fig. 5a). This gave ΔH^0_{ROP} = –10 kJ mol^{-1} and ΔS^0_{ROP} = –20 J K^{-1} mol^{-1}. The enthalpy of ROP for **5** is comparable to that for moderately strained rings such as THF (ΔH^0 = –19 kJ mol^{-1}) and hexamethylcyclotrisiloxane (ΔH^0 = –23 kJ mol^{-1}).[35] The ΔS^0 value is significantly less negative than that of THF (ΔS^0 = –74 J K^{-1} mol^{-1}), and slightly more negative than that of hexamethylcyclotrisiloxane (ΔS^0 = –3 J K^{-1} mol^{-1}).[35] This entropy of ROP is relatively small in magnitude, and is likely a reflection of the conformational flexibility of polymer **7**, which contains metallocene units that exhibit free rotation around the Cp–Ni–Cp axis relative to the constrained ring **5**, and this would partially compensate for the normal loss of translational entropy associated with a polymerization.

Reversible polymerization of [*n*]metallocenophanes has not been previously observed and this report represents the first determination of the entropic term associated with their ROP. At ambient temperatures, the values of ΔH^0_{ROP} and $T\Delta S^0_{ROP}$ for the transformation of **5** to **7** are of similar magnitude. This results in a very small value for ΔG^0_{ROP} (2.5 kJ mol^{-1}) which explains the reversibility detected. Although comparatively little is known about

thermodynamics for the ROP of [*n*]metallocenophanes, ΔH_{ROP} values have been estimated in several cases using differential scanning calorimetry analyses of ROP exotherms. The data supports the assertion that the ROPs are strain driven and values for ΔH_{ROP} range from ca. 130 kJ mol^{-1} (for thia[1]ferrocenophane **8**: tilt angle α = 31.0°),[49] to ca. 12 kJ mol^{-1} (for carba(phenyl)phospha[2]ferrocenophane **9**: α = 15.0°) (Fig. 1e).[50] The carbasila-bridged [2]ferrocenophane **10** (α = 11.8°) is resistant to ROP, presumably due the reduction in strain compared to **8** and **9 (**Fig. 1e).[50] The enthalpy change associated with the ROP of **5** (ΔH^0_{ROP} = –10 kJ mol^{-1}) is similar in value to that for **9** (α = 15.0°), with which it has a comparable tilt angle (16.6°). In the case of **9** reversible ROP does not occur, presumably as a result of the negligible lability of the Fe–Cp bonds.

In order to provide a direct comparison of the "strain" associated with tilt in both ferrocene and nickelocene, calculations of the bending energy of the metallocene Cp rings as a function of tilt angle were performed (Fig. 5b, Supplementary Table 4). As expected, the energy of nickelocene increases with tilting, in a qualitatively similar manner to ferrocene.[51] However, the energy penalty is consistently smaller than that for ferrocene at all calculated values of α. For example, at α = 15°, the total energy of ferrocene is ca. 14 kJ mol^{-1} higher than that of nickelocene, which is presumably manifested in the longer, weaker Ni–Cp bond and the consequential ease of bending about the Cp–Ni–Cp axis. As noted above, the reported experimental ROP exotherm for **9** (ΔH_{ROP} = ca. –12 kJ mol^{-1}) is the same as that calculated for **5** within experimental error. However, it is clear from Fig. 5b that, even though the tilt angles of **5** and **9** may be similar, the total energy increase on tilting is expected to be higher for the ferrocenophane than the nickelocenophane. We assume that the bulkier side groups present on the bridge in **9** compared to those in **5** reduces the observed enthalpy of polymerization to a value close to that for the latter species.

We also investigated the rheological behaviour of polynickelocene **7** in pyridine in order to gain further insight into the static/dynamic behaviour of this material (e.g. complex viscosity, Supplementary Fig. 17). In general, the application of stress to a sample of entangled polymer chains results in relaxation via the diffusion of a singular chain relative to those in close proximity (reptation). In supramolecular polymers, an additional relaxation mechanism, chain scission, is also available and, depending on the relative lifetimes (τ_{break} and τ_{rep}), may dominate the rheological behaviour. The rheology of such solutions can be probed under inert atmosphere using DLS microrheology (see Supplementary Information, section 10 for details). A model for the dynamic properties of worm-like micelles has been developed by Cates,[52] and has recently been applied to reversible coordination polymer networks based on neodymium.[53] The total relaxation time (τ) scales with concentration (C) by an exponent, A (equation 4).

$$\tau \sim C^A \qquad (4)$$

In the reptative regime ($\tau_{break} \gg \tau_{rep}$), A = 1.2, whereas "unbreakable chains" ($\tau_{break} \geq \tau_{rep}$) are characterised by A = 3.4. Obtaining τ for **7** from plots of the elastic and viscous moduli (G' and G'' respectively, Supplementary Fig. 18), the exponent A was found to be ca. 5.5 for polymer **7** (Supplementary Fig. 19 and Supplementary Table 6). The observation of a larger value is likely due to the increase in molecular mass with concentration, and associated increase in reptation tube length, causing τ_{rep} to increase above the expectation based solely on the increased number of entanglements. Furthermore, significant changes in molecular weight are not accounted for by the model,[52] nor are they observed for typical supramolecular polymers, which normally have much larger association constants. These results therefore indicate that **7** behaves as a static polymer on the short rheological timescale (ca. 5 s) at room temperature. This is consistent with the relatively slow rate of polymer chain scission detected in depolymerization experiments (equilibrium is reached after ca. 24 h at 20 °C).

Conclusion

We have found that, as a result of the lability of the Ni–Cp bonds, a main chain polymetallocene based on nickelocene (**7**) behaves as a dynamic species in coordinating and polar solvents, as illustrated by the observation of a reversible equilibrium with the corresponding [3]nickelocenophane monomer **5** and cyclic oligomers $\mathbf{6_x}$. Detailed studies of the equilibrium as a function of temperature have allowed the determination of the key thermodynamic parameters that characterise the ROP process and revealed a small, favourable value of ΔH (–10 kJ mol^{-1}) together with a very small and unfavourable value of ΔS (–20 J K^{-1} mol^{-1}). The former is a consequence of the relatively low energy penalty for tilting nickelocene, evidenced by DFT calculations, whereas the latter appears to be an intrinsic feature of the ROP of metallocenophanes. The virtual free rotation about the metallocene units in the polymer main chain, where the metal centre approximates to a "ball-bearing",[54] may well contribute to the conformational flexibility in the polymer leading to the low ΔS value. The studies also showed that the rate of polymer chain scission is relatively slow, even in polar and coordinating solvents, and this was confirmed by microrheological studies, which indicated that the polynickelocene **7** behaves as a static material on the relatively short rheological timescale at room temperature. Polynickelocene **7** is a rare example of a readily accessible and easily handled soluble magnetic polymetallocene, and further development of this and analogous materials will be of considerable interest with respect to their responsive, magnetic,[29] and redox properties (see Supplementary Figs 20–22). Also of interest will be their dynamic behaviour in the bulk state at moderately elevated temperatures (even ferrocenes undergo Fe–Cp ligand exchange at 250 °C).[55]

Methods

Synthesis of 5. The synthesis of **5** involved a modified literature procedure.[29] The reaction of the ligand $Li_2[(C_5H_4)_2(CH_2)_3]$ with $NiCl_2$ was carried as described, but at 40 °C (vs. –78 °C in the original report), which resulted in the yield increasing from 17% to 44%.

Concentration dependency of the ROP of 5. In an example reaction, **5** (90 mg, 0.393 mmol) was dissolved in d_5-pyridine (0.5 mL) to afford a dark blue solution (0.79 M, sample **7b**). The solution was stirred at room temperature for 24 h (at low concentrations, no colour change was observed, and at higher concentrations a colour change from blue to green was evident). ^{1}H NMR spectra were recorded after 24 h, 48 h and 7 days. ^{1}H NMR (48 h, 500 MHz, d_5-pyridine: δ [peak width at half height] = 266.8 [788 Hz] (**6$_2$**: br s, C_5H_4–C*H*$_2$–CH_2–), 197.3 [511 Hz] (**6$_3$**: br s, C_5H_4–C*H*$_2$–CH_2–), 185.2 [468 Hz] (**6$_4$**: br s, C_5H_4–C*H*$_2$–CH_2–), 181.6 (**6$_5$**: overlapping br s, C_5H_4–C*H*$_2$–CH_2–), 176.9 [435 Hz] (**7**: br s, C_5H_4–C*H*$_2$–CH_2–), 9.6 [140 Hz] (**7**: br s, C_5H_4–CH_2–C*H*$_2$–), –29.0 [212 Hz] (**5**: br s, C_5H_4–CH_2–C*H*$_2$–), –245.4 [704 Hz] (**5**: br s, α-C_5H_4), –250.0 [1207 Hz] (**7**: br s, C_5H_4), –270.9 [836 Hz] (**5**: br s, β-C_5H_4) ppm.

Polymeric material was isolated in the cases of **7a**, **7b** and **7c** (1.31, 0.79 and 0.44 M initial monomer concentration respectively) via precipitation of the polymerization solution (0.5 mL) into rapidly stirred hexanes (30 mL). The green solid was isolated, dissolved in a minimum volume of THF (0.5 mL), and quickly precipitated again into hexanes (30 mL). The precipitate was isolated and dried *in vacuo* to yield green polymeric material in yields of 62, 30 and 21% respectively for **7a**, **7b** and **7c**.

The supernatant solution of the first precipitation of **7c** revealed an increase in proportion of cyclic oligomers. ^{1}H NMR (500 MHz, d_5-pyridine/hexanes: δ [peak width at half height] = 266.9 [709 Hz] (**6$_2$**: br s, C_5H_4–C*H*$_2$–CH_2–), 197.1 [412 Hz] (**6$_3$**: br s, C_5H_4–C*H*$_2$–CH_2–),

184.8 [334 Hz] (**6$_4$**: br s, C_5H_4–CH_2–CH_2–), 181.3 [276 Hz] (**6$_5$**: br s, C_5H_4–CH_2–CH_2–), 180.0 (**6$_6$**: overlapping br s, C_5H_4–CH_2–CH_2–), 179.4 (**6$_7$**: overlapping br s, C_5H_4–CH_2–CH_2–), 178.9 (**6$_8$**: overlapping br s, C_5H_4–CH_2–CH_2–), 177.0 (**7**: overlapping br s, C_5H_4–CH_2–CH_2–),. ESI-MS (positive mode): *m/z* 228.0443 [**5**]$^+$, 456.0895 [**6$_2$**]$^+$, 684.1345 [**6$_3$**]$^+$, 912.1796 [**6$_4$**]$^+$.

Temperature dependency of the ROP of 5. In an example experiment **5** (50 mg, 0.219 mmol) was dissolved in deuterated pyridine (0.5 mL) to afford a dark blue solution of concentration 0.44 M, and added to an NMR tube. The sample was held at the desired temperature for 24 h and then a ^{1}H NMR spectrum was recorded at that temperature. ^{1}H NMR (500 MHz, d_5-pyridine, data provided at 5 °C): δ [peak width at half height] = 288.3 [1085 Hz] (**6$_2$**), 210.7 [660 Hz] (**6$_3$**), 197.1 [570 Hz] (**6$_4$**), 188.0 [655 Hz] (**7**: br s, C_5H_4–CH_2–CH_2–), 10.2 [213 Hz] (**7**: br s, C_5H_4–CH_2–CH_2–), –31.4 [591 Hz] (**5**: br s, C_5H_4–CH_2–CH_2–), –264.0 [1074 Hz] (**5**: br s, α-C_5H_4), –268.7 [1041 Hz] (**7**: br s, C_5H_4), –291.37 [1121 Hz] (**5**: br s, β-C_5H_4) ppm.

Additional Information

The authors declare no competing financial interests. Supplementary Information accompanies this paper at xxxx. Reprints and permission information is available online at xxxx. Correspondence and requests for materials should be addressed to I.M.

Data Availability

All data is available from https://data.bris.ac.uk/data or by request from the corresponding author.

Acknowledgements

R.A.M., A.D.R., G.R.W. and I.M. thank the EPSRC for funding. D.W.H. is supported by EPSRC doctoral training centre grant [EP/G036780/1]. The authors would like to thank Dr Ben MacCreath for assistance in performing DLS microrheology measurements.

Author contributions

R.A.M., A.D.R. and I.M. devised the project. R.A.M. carried out the experiments with assistance from A.D.R.. The SAXS data was collected and analysed by D.W.H.. Microrheology experiments were performed by R.A.M. and G.R.W.. Paramagnetic NMR experiments were designed with assistance from P.G.L, mass spectrometry was performed by P.J.G., and computational chemistry was performed by J.C.G. The manuscript was written by R.A.M. with input from A.D.R., G.R.W. and I.M. The project was supervised by I.M. with input from G.R.W.

References

1. Whittell, G. R., Hager, M. D., Schubert, U. S., Manners, I. Functional soft materials from metallopolymers and metallosupramolecular polymers. *Nat. Mater.* **10,** 176-188 (2011).

2. Xiang, J., Ho, C. L., Wong, W. Y. Metallopolymers for energy production, storage and conservation. *Polym. Chem.* **6,** 6905-6930 (2015).

3. Yan, Y., Zhang, J., Ren, L., Tang, C. Metal-containing and related polymers for biomedical applications. *Chem. Soc. Rev.* **45**, 5232-5263 (2016).

4. De Greef, T. F. A. *et al.* Supramolecular polymerization. *Chem. Rev.* **109,** 5687-5754 (2009).

5. Yang, L., Tan, X., Wang, Z., Zhang, X. Supramolecular polymers: Historical development, preparation, characterization, and functions. *Chem. Rev.* **115,** 7196-7239 (2015).

6. Burnworth, M. *et al.* Optically healable supramolecular polymers. *Nature* **472,** 334-337 (2011).

7. Bode, S., *et al.* Self-healing polymer coatings based on crosslinked metallosupramolecular copolymers. *Adv. Mater.* **25,** 1634-1638 (2013).

8. Wu, F.-I. *et al.* Efficient white-electrophosphorescent devices based on a single polyfluorene copolymer. *Adv. Funct. Mater.* **17,** 1085-1092 (2007).

9. Stanley, J. M., Holliday, B. J. Luminescent lanthanide-containing metallopolymers. *Coord. Chem. Rev.* **256,** 1520-1530 (2012).

10. Tse, C. W., *et al.* Layer-by-layer deposition of rhenium-containing hyperbranched polymers and fabrication of photovoltaic cells. *Chem. Eur. J.* **13,** 328-335 (2007).

11. Wong, W.-Y., Ho, C.-L. Organometallic photovoltaics: A new and versatile approach for harvesting solar energy using conjugated polymetallaynes. *Acc. Chem. Res.* **43,** 1246-1256 (2010).

12. Kim, H.-J., Lee, J.-H., Lee, M. Stimuli-responsive gels from reversible coordination polymers. *Angew. Chem. Int. Ed.* **44,** 5810-5814 (2005).

13. Astruc, D., Ornelas, C., Ruiz, J. Metallocenyl dendrimers and their applications in molecular electronics, sensing, and catalysis. *Acc. Chem. Res.* **41,** 841-856 (2008).

14. Collot, J. *et al.* Artificial metalloenzymes for enantioselective catalysis based on biotin-avidin. *J. Am. Chem. Soc.* **125,** 9030-9031 (2003).

15. Choi, T.-L. *et al.* Synthesis and nonvolatile memory behavior of redox-active conjugated polymer-containing ferrocene. *J. Am. Chem. Soc.* **129,** 9842-9843 (2007).

16. Zhang, J., *et al.* Antimicrobial metallopolymers and their bioconjugates with conventional antibiotics against multidrug-resistant bacteria. *J. Am. Chem. Soc.* **136,** 4873-4876 (2014).

17. Rider, D. A., *et al.* Nanostructured magnetic thin films from organometallic block copolymers: Pyrolysis of self-assembled polystyrene-*block*-poly(ferrocenylethylmethylsilane). *ACS Nano* **2,** 263-270 (2008).

18. Korczagin, I., Lammertink, R. G. H., Hempenius, M. A., Golze, S., Vancso, G. J. Surface nano- and microstructuring with organometallic polymers. *Adv. Polym. Sci.* **200,** 91-117 (2006).

19. Wang, Y. L., Salmon, L., Ruiz, J., Astruc, D. Metallodendrimers in three oxidation states with electronically interacting metals and stabilization of size-selected gold nanoparticles. *Nat. Commun.* **5,** 1-12 (2014).

20. Herbert, D. E., Mayer, U. F. J., Manners, I. Strained metallocenophanes and related organometallic rings containing π-hydrocarbon ligands and transition-metal centers. *Angew. Chem. Int. Ed.* **46,** 5060-5081 (2007).

21. Musgrave, R. A., Russell, A. D., Manners, I. Strained Ferrocenophanes. *Organometallics* **32,** 5654-5667 (2013).

22. Braunschweig, H., Kupfer, T. Non-iron [*n*]metalloarenophanes. *Acc. Chem. Res.* **43,** 455-465 (2010).

23. Tamm, M. Synthesis and reactivity of functionalized cycloheptatrienyl-cyclopentadienyl sandwich complexes. *Chem. Commun.* 3089-3100 (2008).

24. Bhattacharjee, H., Müller, J. Metallocenophanes bridged by group 13 elements. *Coord. Chem. Rev.* **314,** 114-133 (2016).

25. Mayer, U. F. J., Gilroy, J. B., O'Hare, D., Manners, I. Ring-opening polymerization of 19-electron [2]cobaltocenophanes: A route to high-molecular-weight, water-soluble polycobaltocenium polyelectrolytes. *J. Am. Chem. Soc.* **131,** 10382-10383 (2009).

26. Qiu, H., Gilroy, J. B., Manners, I. DNA-induced chirality in water-soluble poly(cobaltoceniumethylene). *Chem. Commun.* **49,** 42-44 (2013).

27. Braunschweig, H. *et al.* Synthesis of a paramagnetic polymer by ring-opening polymerization of a strained [1]vanadoarenophane. *Angew. Chem., Int. Ed.* **47,** 3826-3829 (2008).

28. Braunschweig, H. *et al.* A paramagnetic heterobimetallic polymer: Synthesis, reactivity, and ring-opening polymerization of tin-bridged homo- and heteroleptic vanadoarenophanes. *J. Am. Chem. Soc.* **137,** 1492-1500 (2015).

29. Baljak, S. *et al.* Ring-opening polymerization of a strained [3]nickelocenophane: A route to polynickelocenes, a class of S=1 metallopolymers. *J. Am. Chem. Soc.* **136,** 5864-5867 (2014).

30. Long, N. J. *Metallocenes: An introduction to sandwich complexes* (Wiley-Blackwell, Oxford, 1998).

31. Tel'noi, V. I., Rabinovich, I. B. Thermochemistry of organic compounds of transition metals. *Russ. Chem. Rev.* **46,** 1337-1367 (1977).

32. Inkpen, M. S., *et al.* Oligomeric ferrocene rings. *Nature Chem.* **8,** 825-830 (2016).

33. Herbert, D. E., *et al.* Redox-active metallomacrocycles and cyclic metallopolymers: Photocontrolled ring-opening oligomerization and polymerization of silicon-bridged [1]ferrocenophanes using substitutionally-labile lewis bases as initiators. *J. Am. Chem. Soc.* **131,** 14958-14968 (2009).

34. Semlyen, J. A. Ring-chain equilibria and the conformations of polymer chains. *Adv. Polym. Sci.* **21,** 41-75 (1976).

35. Duda, A., Kowalski, A. *Handbook of Ring-opening Polymerization*, Chapter 1 (Wiley-VCH Verlag GmbH & Co., Weinheim, 2009).

36. Ohta, H. *et al.* A N-heterocyclic carbene Ni(II) complex bearing bis(cyclopentadienyl) ligands as a precatalyst for the dehydrogenative silylation of alcohols with hydrosilanes. *Tetrahedron Lett.* **56,** 2910-2912 (2015).

37. Cross, R. J., Wardle, R. Cyclopentadienyls of palladium and platinum. *J. Chem. Soc. A*, 2000-2007 (1971).

38. Herberich, G. E., Hausmann, I., Hessner, B., Negele, M. Dehydrating complex-formation of borolenes with (cyclopentadienyl)nickel complexes. *J. Organomet. Chem.* **362,** 259-264 (1989).

39. Heinicke, J. *et al.* Metalated 1,3-azaphospholes: η^1-(1*H*-1,3-benzazaphosphole-*P*)M(CO)$_5$ and μ_2-[(1,3-benzazaphospholide-*P*)(cyclopentadienide)nickel] complexes. *Z. Anorg. Allg. Chem.* **628,** 2869-2876 (2002).

40. Kuhn, N., Winter, M., Zimmer, E. Coordination of trifunctional phosphane ligands in cyclopentadienylnickel complexes. *J. Organomet. Chem.* **344,** 401-409 (1988).

41. Odian, G. *Principles of Polymerization*, Chapter 7 (John Wiley & Sons, New Jersey, 2004).

42. Chu, B., Hsiao, B. S. Small-angle X-ray scattering of polymers. *Chem. Rev.* **101,** 1727-1761 (2001).

43. Wall, L. A. Energetics of polymer decompositions. II. *Soc. Plastic Eng. J.* **16,** 1031-1035 (1960).

44. Wall, L. A. Polymer decomposition: Thermodynamics, mechanisms, and energetics. *Soc. Plastic Eng. J.* **16,** 810-814 (1960).

45. McCormick, H. W. Ceiling temperature of alpha-methylstyrene. *J. Polym. Sci.* **25,** 488-490 (1957).

46. Cook, R. E., Dainton, F. S., Ivin, K. J. Effect of structure on polymerizability - Olefin polysulfone formation. *J. Polym. Sci.* **29,** 549-556 (1958).

47. Tuba, R., Grubbs, R. H. Ruthenium catalyzed equilibrium ring-opening metathesis polymerization of cyclopentene. *Polym. Chem.* **4,** 3959-3962 (2013).

48. Kubisa, P., Penczek, S. Cationic activated monomer polymerization of heterocyclic monomers. *Prog. Polym. Sci.* **24,** 1409-1437 (1999).

49. Rulkens, R. *et al.* Highly strained, ring-tilted [1]ferrocenophanes containing group 16 elements in the bridge: synthesis, structures, and ring-opening oligomerization and polymerization of [1]thia- and [1]selenaferrocenophanes. *J. Am. Chem. Soc.* **119,** 10976-10986 (1997).

50. Resendes, R. *et al.* Tuning the strain and polymerizability of organometallic rings: the synthesis, structure, and ring-opening polymerization behavior of [2]ferrocenophanes with C–Si, C–P, and C–S bridges. *J. Am. Chem. Soc.* **123,** 2116-2126 (2001).

51. Green, J. C. Bent metallocenes revisited. *Chem. Soc. Rev.* **27,** 263-271 (1998).

52. Turner, M. S., Marques, C., Cates, M. E. Dynamics of wormlike micelles: The "bond-interchange" reaction scheme. *Langmuir* **9,** 695-701 (1993).

53. Vermonden, T. *et al.* Linear rheology of water-soluble reversible neodymium(III) coordination polymers. *J. Am. Chem. Soc.* **126,** 15802-15808 (2004).

54. Li, C. *et al.* Neutral molecule receptor systems using ferrocene's "atomic ball bearing" character as the flexible element. *J. Am. Chem. Soc.* **119,** 1609-1618 (1997).

55. Allcock, H. R., McDonnell, G. S., Riding, G. H., Manners, I. Influence of different organic side groups on the thermal behavior of polyphosphazenes: Random chain cleavage, depolymerization, and pyrolytic cross-linking. *Chem. Mater.* **2,** 425-432 (1990).

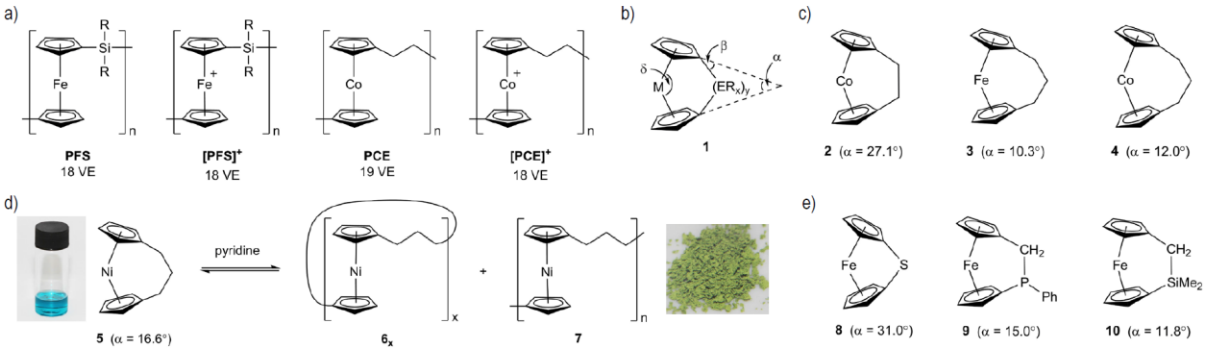

Figure 1. Summary of monomer [*n*]metallocenophanes and polymetallocenes. a) Examples of diamagnetic and paramagnetic main chain polymetallocenes based on iron and cobalt: polyferrocenylsilane (PFS) and polycobaltocenylethylene (PCE). b) Geometric parameters that characterize the structural distortions, and hence the ring strain, in [*n*]metallocenophanes (α = dihedral angle between the plane of each Cp ring, β = [180° – (Cp_{cent}–C_{ipso}–Si angle)], δ = Cp_{cent}–Fe–Cp'_{cent} angle). c) Hydrocarbon-bridged [*n*]cobaltocenophanes and [*n*]ferrocenophanes, showing the effect of the nature of the bridging moiety and M–Cp bond on the degree of Cp ring tilt. d) Reversible polymerization of tricarba[3]nickelocenophane monomer **5** (blue solution) to yield cyclic oligomers $\mathbf{6_x}$, and polynickelocene **7** (isolated as a green solid). e) Examples of [*n*]ferrocenophanes with various ansa-bridging moieties and their respective tilt angles.

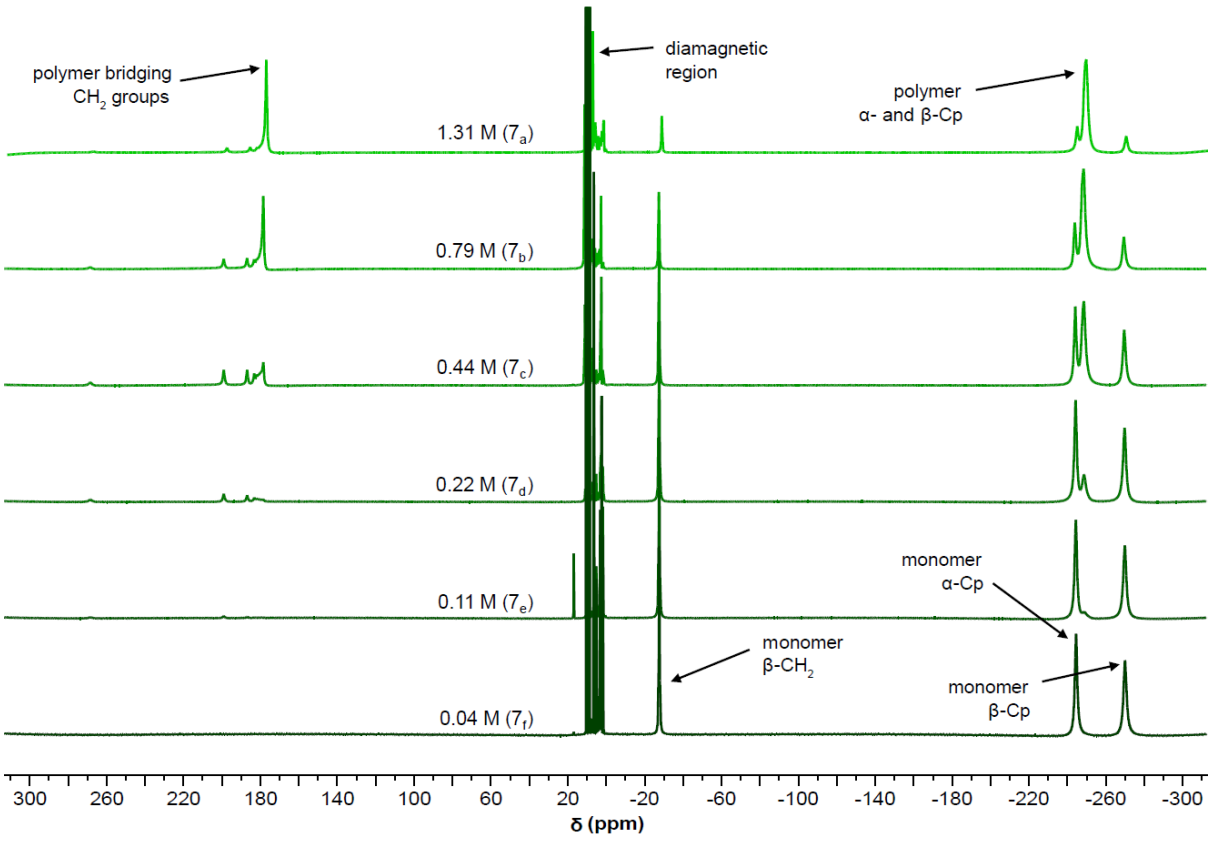

Figure 2. Stacked ^{1}H NMR spectra (500 MHz, d_5-pyridine, 25 °C) showing the effect of initial monomer concentration on the conversion of tricarba[3]nickelocenophane monomer **5** to polynickelocene **7**. ^{1}H NMR spectra of a range of initial concentrations of **5** from 0.04 to 1.31 M (t = 48 h, 25 °C) are shown, and resonances of the cyclopentadienyl and bridging CH_2 groups are labelled for monomer **5** and polymer **7**. At low concentrations, there is negligible conversion to polymer, and as concentration increases, the conversion to polymer also increases (for effect of concentration on the yield of **7** see Table 1).

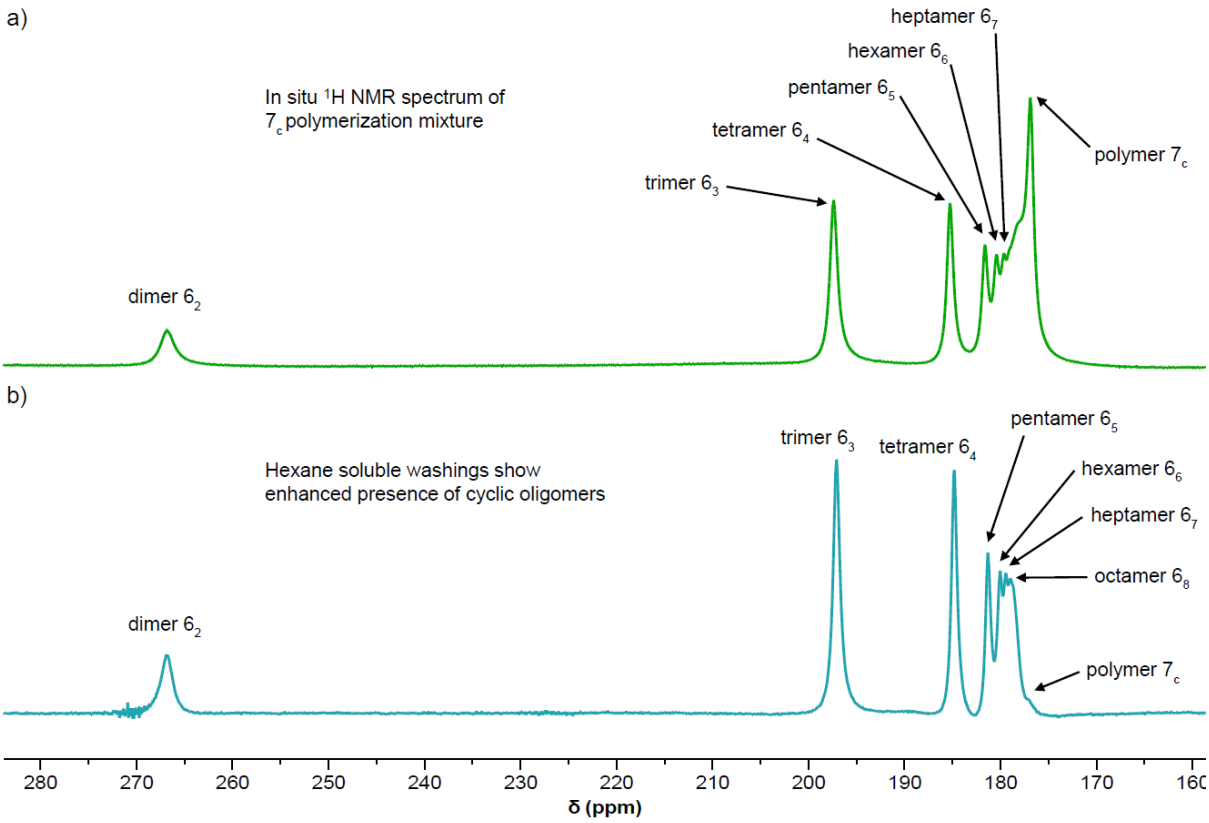

Figure 3. Example ^{1}H NMR spectra showing the presence of cyclic oligomers **6$_x$** in equilibrium mixtures of monomer **5** and polymer **7**. a) Selected region of ^{1}H NMR spectrum (500 MHz, d_5-pyridine, 25 °C) of polymerization mixture for **7$_c$** (0.44 M, d_5-pyridine, 24 h), showing the resonance of bridging C_5H_4–CH_2–CH_2 groups in polymer **7$_c$** and a number of cyclic oligomers **6$_x$** (x = 2–8) with the resonance corresponding to each oligomer decreasing in value with increasing degree of oligomerization (x). b) Selected region of ^{1}H NMR spectrum of supernatant from the polymerization mixture for **7$_c$** (500 MHz, d_5-pyridine/hexanes) after removal of sufficiently high molecular weight polymeric material by precipitation once into hexanes, showing enhanced resonances assigned to cyclic species.

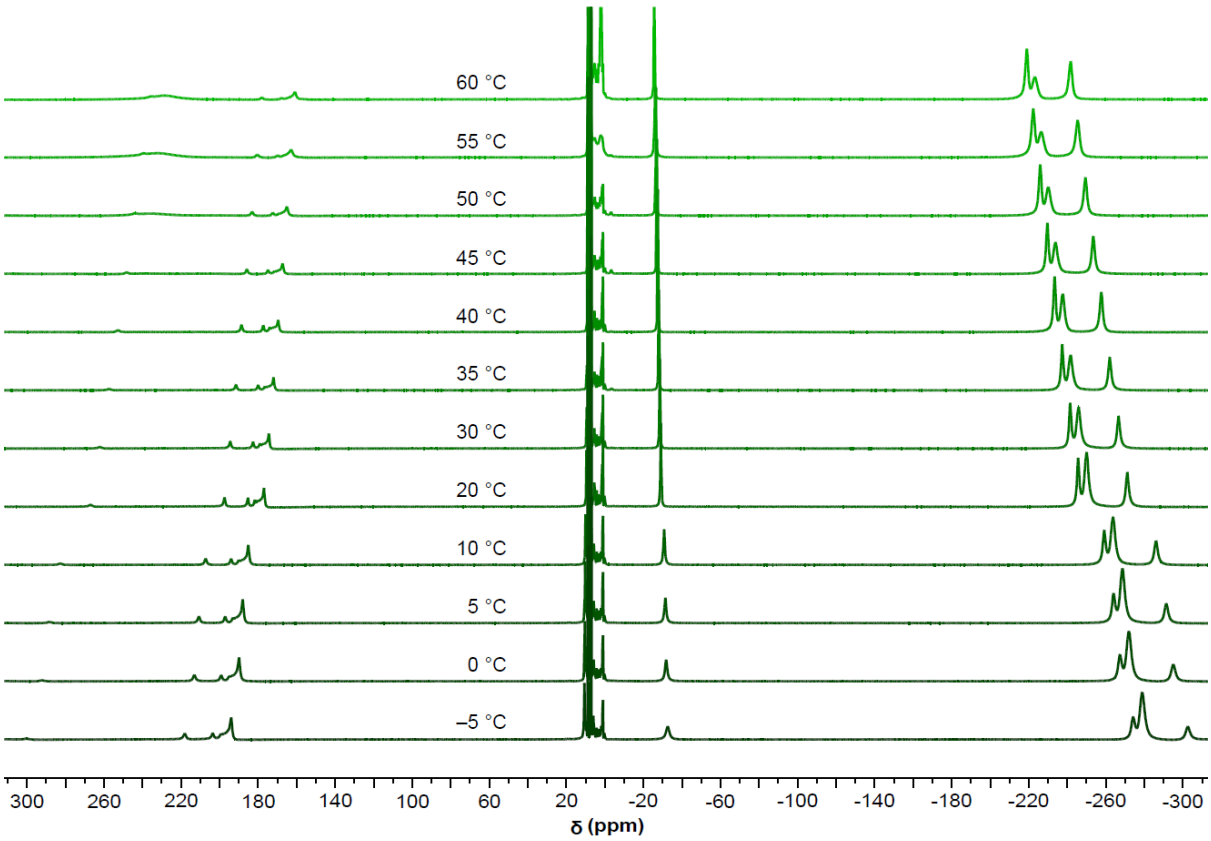

Figure 4. Stacked ^{1}H NMR spectra (500 MHz, d_5-pyridine) showing the effect of temperature on the reversible conversion of monomer **5** to polymer **7** (initial monomer concentration = 0.44 M, t = 24 h). Within the equilibrium mixture, polymer **7** is favoured at lower temperatures.

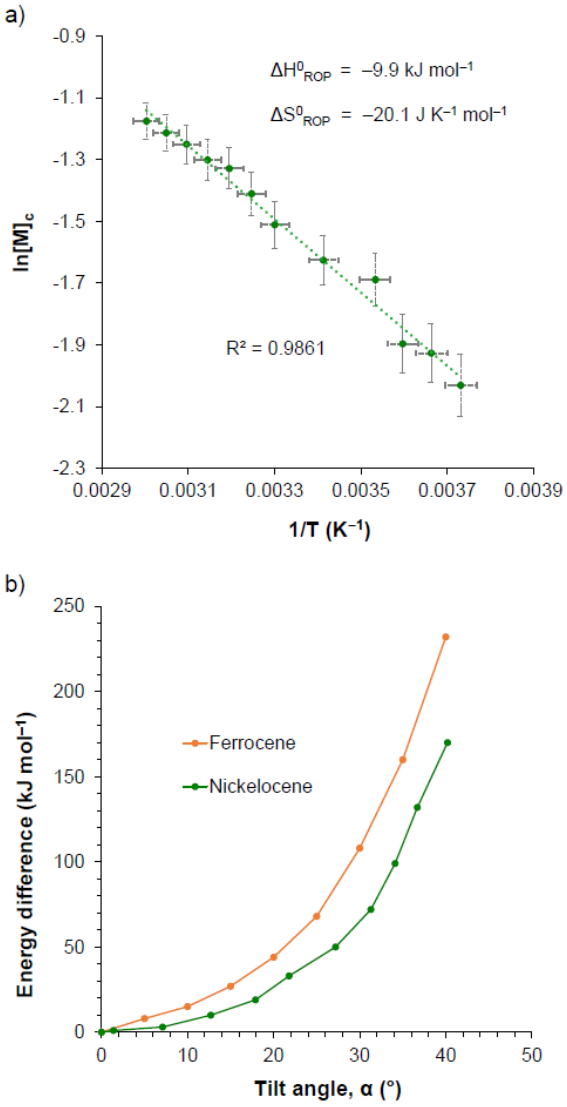

Figure 5. Influence of metallocene ring tilt on thermodynamic parameters characterising ring-opening processes in [*n*]metallocenophanes. a) Van't Hoff plot showing the relationship between $\log_e$ of the equilibrium monomer concentration and reciprocal temperature for the ROP of **5**, with enthalpic and entropic parameters for the polymerisation displayed (see Supplementary Table 3). b) Variation of the total energy of ferrocene and nickelocene as a function of the tilt angle (α), derived by computational methods (Supplementary Table 4).

Sample	Conc. (M)	% of **7** (^{1}H NMR)			Yield of **7** (%)[a]	DLS[e]			SAXS[h]
		24 h	48 h	7 days	(at 32 h)	R_h (nm)	σ[f]	M_w (g mol^{-1})[g]	M_w (g mol^{-1})[i]
7$_a$	1.31	79.2	78.9	78.6	62	5.7[c]	3.8	50,900[g]	[j]
7$_b$	0.79	68.5	69.0	71.0	30	6.3[c]	5.0	61,200[g]	20,000[k]
7$_c$	0.44	43.5	48.5	47.6	21	3.2[d]	2.9	17,600[g]	6,400[k]
7$_d$	0.22	13.0	20.6	24.8	[b]	–	–	–	–
7$_e$	0.11	2.9	4.3	10.7	[b]	–	–	–	–
7$_f$	0.04	2.9	2.9	4.8	[b]	–	–	–	–

Table 1. Effect of initial monomer concentration on conversion of monomer **5** to polymer **7** at room temperature (ca. 20 °C) in d_5-pyridine. [a]Isolated yield (via two precipitations of polymer solution into hexanes, then drying *in vacuo*). [b]No polymer could be isolated via precipitation into hexanes. [c]Polymer only partially soluble in toluene at 1 mg mL^{-1}. [d]Polymer fully soluble in toluene at 1 mg mL^{-1}. [e]DLS experiments carried out on toluene solutions of polymers. [f]Standard deviation across DLS measurements. [g]Estimated in toluene by means of calibration with R_h/M_w correlations for poly(ferrocenyldimethylsilane) in THF. [h]Scattering experiments carried out on toluene solutions of polymers. [i]Calculated using polymer density, D_P = 1.26 g cm^{-3}. [j]Solubility of **7$_a$** in toluene too low to allow for sufficient scattering intensity. [k]Absolute value of M_w determined in toluene.